Optical Engineering

OpticalEngineering.SPIEDigitalLibrary.org

Fano resonance in asymmetric-period two-dimensional plasmonic absorbers for dual-band uncooled infrared sensors

Shinpei Ogawa
Yousuke Takagawa
Masafumi Kimata

Shinpei Ogawa, Yousuke Takagawa, Masafumi Kimata, "Fano resonance in asymmetric-period two-dimensional plasmonic absorbers for dual-band uncooled infrared sensors," *Opt. Eng.* **55**(11), 117105 (2016), doi: 10.1117/1.OE.55.11.117105.

Optical Engineering 55(11), 117105 (November 2016)

Fano resonance in asymmetric-period two-dimensional plasmonic absorbers for dual-band uncooled infrared sensors

Shinpei Ogawa,[a,*] Yousuke Takagawa,[b] and Masafumi Kimata[b]
[a]Mitsubishi Electric Corporation, Advanced Technology R&D Center, 8-1-1 Tsukaguchi-Honmachi, Amagasaki, Hyogo 661-8661, Japan
[b]Ritsumeikan University, College of Science and Engineering, 1-1-1 Noji-higashi, Kusatsu, Shiga 525-8577, Japan

Abstract. The spectral discrimination function of uncooled infrared (IR) sensors has significant advantages for applications such as fire detection, gas analysis, and biological analysis. We have previously demonstrated wavelength-selective uncooled IR sensors using two-dimensional plasmonic absorbers (2-D PLAs) over a wide range spanning the middle- and long-wavelength IR regions. 2-D PLAs are highly promising in terms of practical application due to the ease of fabrication and robustness for structural fluctuations. However, dual-band operation based on this concept has not yet been investigated, even though the ability to absorb in two different wavelength bands is extremely important for object recognition. Thus, a dual-band uncooled IR sensor was developed that employs Fano resonance in the plasmonic structures. To achieve dual-band detection, asymmetric periods in the orthogonal x- and y-directions were introduced into 2-D PLAs. Theoretical investigations predicted an asymmetric absorbance line shape dependent on the polarization attributed to Fano resonance. The spectral responsivity of the developed sensor demonstrated that selective detection occurred in two different wavelength bands due to polarization-dependent Fano resonance. The results obtained in this study will be applicable to the development of advanced sensors capable of multiband detection in the IR region.
 [DOI: 10.1117/1.OE.55.11.117105]

Keywords: Fano resonance; plasmonics; metamaterial; uncooled infrared sensors; dual-band.

Paper 161334P received Aug. 25, 2016; accepted for publication Oct. 31, 2016; published online Nov. 22, 2016; corrected Nov. 23, 2016.

1 Introduction

There has been growing interest in uncooled infrared (IR) sensors[1] in both industry and the field of applied physics.[2] Typical uncooled IR sensors can detect information such as the average radiant intensity, position, and shape of an object. If uncooled IR sensors could obtain wavelength information, then objects could be identified through their radiation spectrum.[3] Wavelength-selectivity in IR sensors could also lead to additional applications, including gas analysis, fire detection, hazardous materials recognition, and ultimately multicolor information. However, there has been serious difficulty to date in the construction of pixel-array formats with different detection wavelengths using typical wavelength-selective methods such as filters[4–7] or optical resonant cavities.[8] Additional optical attachments such as filters lead to complicated systems, which in turn leads to higher costs and a degeneration of the wavelength selectivity because the filters themselves emit IR radiation. Our group has developed advanced functional uncooled IR sensors with wavelength selectivity,[9,10] multicolor imaging,[11] or polarization selectivity[12,13] using plasmonics[14,15] and metamaterials[16,17] technologies to address this challenge and expand the potential applications. Absorbers that employ plasmonic and metamaterials have the advantage of enabling control over the absorption wavelength simply by varying the surface structural design. This has led to the fabrication of array formats with different detection wavelengths without the need for any filters or optical attachments, and thus the realization of low-cost and high-spectral selectivity systems.

Although we have realized single-mode operation, dual-band detection has not yet been investigated. Dual-band operation is particularly important with regard to analytical sensing applications, such as gas and material sensing as one potential use. Metal–insulator–metal absorbers[18,19] are good candidates for this type of dual-band operation;[20,21] however, such structures have restrictions in terms of the operation wavelength range[22] and require precise control over the metal patch size[23] for control of the absorption wavelength, which leads to complex manufacturing procedures and thus increases cost. On the other hand, two-dimensional plasmonic absorbers (2-D PLAs) have rich potential for a variety of practical applications due to their wide operational range in the middle- and long-wavelength IR regions, in addition to their simple fabrication processes and structural robustness.[10,24,25]

We have recently reported 2-D PLAs with asymmetric periods (2-D PLA-APs) that realize dual-band operation due to Fano resonance.[26] Fano resonance is a phenomenon that involves interference between a discrete state and a continuum state.[27,28] Recently, Fano resonance has been identified in various metallic photonic,[29,30] plasmonic, and metamaterial structures.[31–33] However, the detailed effect of Fano resonance in 2-D PLA-APs for dual-band detection has not yet been reported. Here, we provide a detailed report on dual-band detection based on Fano resonance induced in the asymmetric geometry of 2-D PLA-APs.

*Address all correspondence to: Shinpei Ogawa, E-mail: Ogawa. Shimpei@eb.MitsubishiElectric.co.jp

2 Theoretical Design

Figure 1(a) shows a schematic illustration of a symmetric Au-based 2-D PLA. Figures 1(b) and 1(c) show the top views of 2-D PLAs with symmetric and asymmetric periods, respectively. Figure 1(d) shows the definition of the polarization angle (θ) for the incident electric wave (E). In this study, the incident angle was normal to the surface, considering practical applications. It should be noted that Figs. 1(b) and 1(c) show only four unit cells, where the periods p_x and p_y are defined in the x- and y-directions, along with the diameter, d.

The p_x, p_y, and d values, and the depth of the dimples were set at 6.5, 4.0, 3.0, and 1.5 μm for both calculations and experimental trials, considering the resolution limit of the experimental instrumentation and for comparison with our previous studies. The absorption wavelength of symmetric 2-D PLAs maintains a single mode, is independent of the polarization, and is almost equal to the surface period, as demonstrated previously.[10,12] The absorption properties of the 2-D PLA-AP were calculated using rigorous coupled wave analysis (RCWA). Figure 2 shows the absorbance spectra for nonpolarization and for θ at 0 deg and 90 deg. The spectrum for nonpolarization was calculated using θ at 45 deg, which can be obtained from the average of the spectra for θ at 0 deg and 90 deg.

Figure 2 indicates that the strong polarization dependence is produced due to the symmetry-broken period structures. Two absorption peaks of approximately 40% and 50% are observed for nonpolarization, and of approximately 35% and 90% for $\theta = 0$ deg at approximately 4.0 and 6.5 μm, which almost correspond to p_y and p_x, respectively. The asymmetric line shape of Fano resonance is evident in these spectra. In contrast, only a single and broad absorption peak of 50% is observed for $\theta = 90$ deg at around 4.0 μm, which corresponds to p_y. These results indicate that dual-absorption peaks are produced due to the interference of the surface plasmon modes in the x and y period for $\theta = 0$ deg, while the single absorption peak for $\theta = 90$ deg

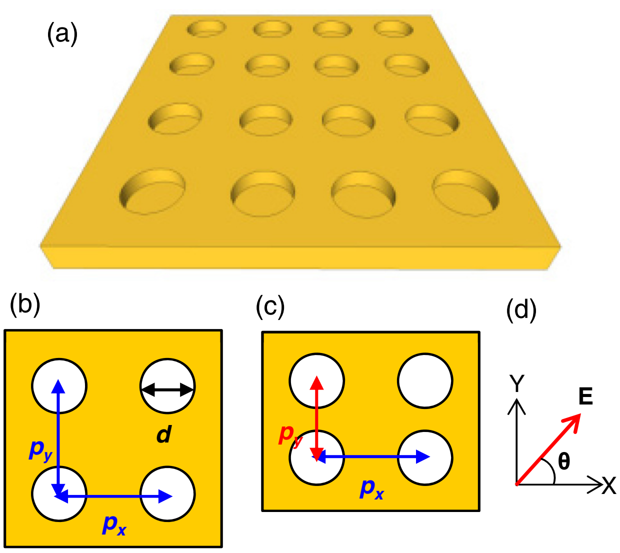

Fig. 1 (a) Schematic diagram of a symmetric 2-D PLA. Structural dimensions of 2-D PLAs with (b) symmetric and (c) asymmetric periods. (d) Definition of the electric field polarization angle (θ).

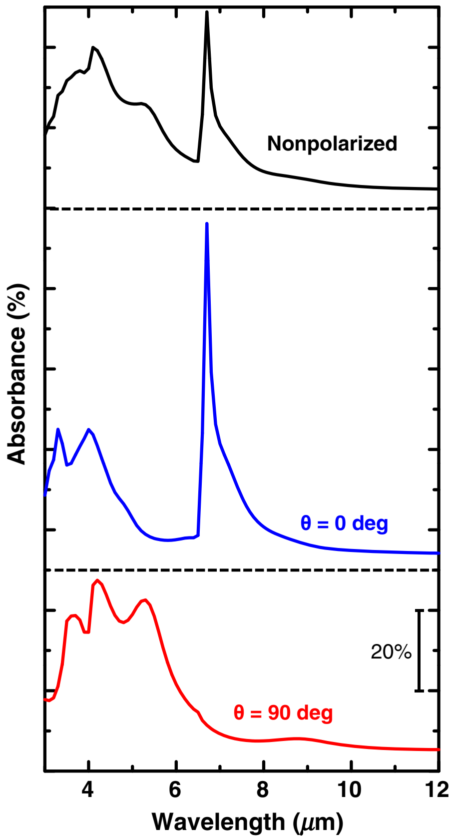

Fig. 2 Absorbance spectra for nonpolarization and θ at 0 deg and 90 deg. The scale bar represents 20%.

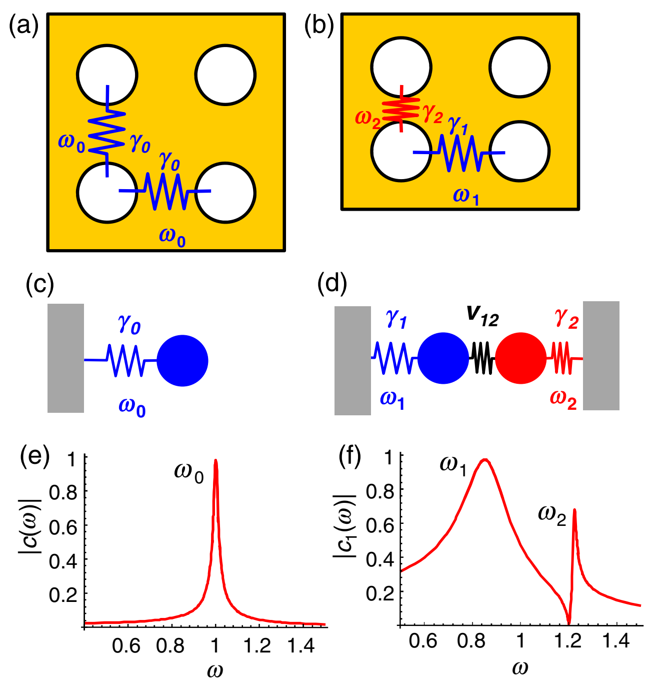

Fig. 3 Classical analogy of Fano resonance for (a) symmetric and (b) asymmetric period 2-D PLAs. (c) Single and (d) double oscillator models. (e) Normalized oscillation amplitude of $c(\omega)$ in the single oscillator model. (f) Normalized oscillation amplitude of $c_1(\omega)$ in the double oscillator model.

is attributed to the surface plasmon mode only in the y-direction. The surface plasmon wavelength in the x-direction is longer than that in the y-direction; therefore, these two resonances can interfere only for $\theta = 0$ deg. On the other hand, there is less interference of these two modes in the y-direction.

These properties were investigated in detail by applying the classical analogy of Fano resonance[28] to 2-D PLA-APs. The surface plasmon resonances in the x- and y-directions are the same in symmetric 2-D PLAs due to the symmetric geometry, whereas they are different in 2-D PLA-APs due to the asymmetric geometry, as shown in Fig. 2. Therefore, symmetric and asymmetric-period 2-D PLAs can be considered with respect to single and double oscillator models, as schematically shown in Figs. 3(a) and 3(c), and in 3(b) and 3(d), respectively.

ω_0 is the natural frequency of the oscillator, which is defined by the mass and the spring constant in the absence of damping, and γ_0 is the frictional parameter. ω_1 and ω_2 are the natural frequencies of the oscillator for the x- and y-directions, γ_1 and γ_2 are the frictional parameters for the x- and y-directions, and ν_{12} is the coupling of the two oscillators. The oscillation amplitude $c(\omega)$ for the single oscillator and $c_1(\omega)$ and $c_2(\omega)$ for the double oscillator are described in Ref. 28, as follows:

$$|c(\omega)| = \frac{A}{\sqrt{(\omega_0^2 - \omega^2)^2 + \omega^2\gamma^2}}, \tag{1}$$

$$|c_1(\omega)| = \left| \frac{\omega_2^2 - \omega^2 + j\gamma_2\omega}{(\omega_1^2 - \omega^2 + j\gamma_1\omega)(\omega_2^2 - \omega^2 + j\gamma_2\omega) - \nu_{12}^2} A_1 \right|, \tag{2}$$

$$|c_2(\omega)| = \left| \frac{\nu_{12}}{(\omega_1^2 - \omega^2 + j\gamma_1\omega)(\omega_2^2 - \omega^2 + j\gamma_2\omega) - \nu_{12}^2} A_1 \right|, \tag{3}$$

where A and A_1 are the constants. We focus on Eqs. (1) and (2) to investigate the asymmetric line shape. Figures 3(e) and 3(f) show the results calculated for Eqs. (1) and (2), respectively, using $\omega_0 = 1.0$ and $\gamma = 0.02$ in Eq. (1), and $\omega_1 = 0.8$, $\omega_2 = 1.2$, $\gamma_1 = 0.02$, $\gamma_2 = 0$, and $\nu_{12} = 0.2$ in Eq. (2). Both results were normalized according to the peak value.

These results show that the single and double oscillator models have single and dual resonance peaks, which correspond to the absorption properties of symmetric 2-D PLAs and 2-D PLA-APs, respectively. The single resonance peak as shown in Fig. 3(e) and the first resonance peak as shown in Fig. 3(f) were symmetric. These resonances can be fitted

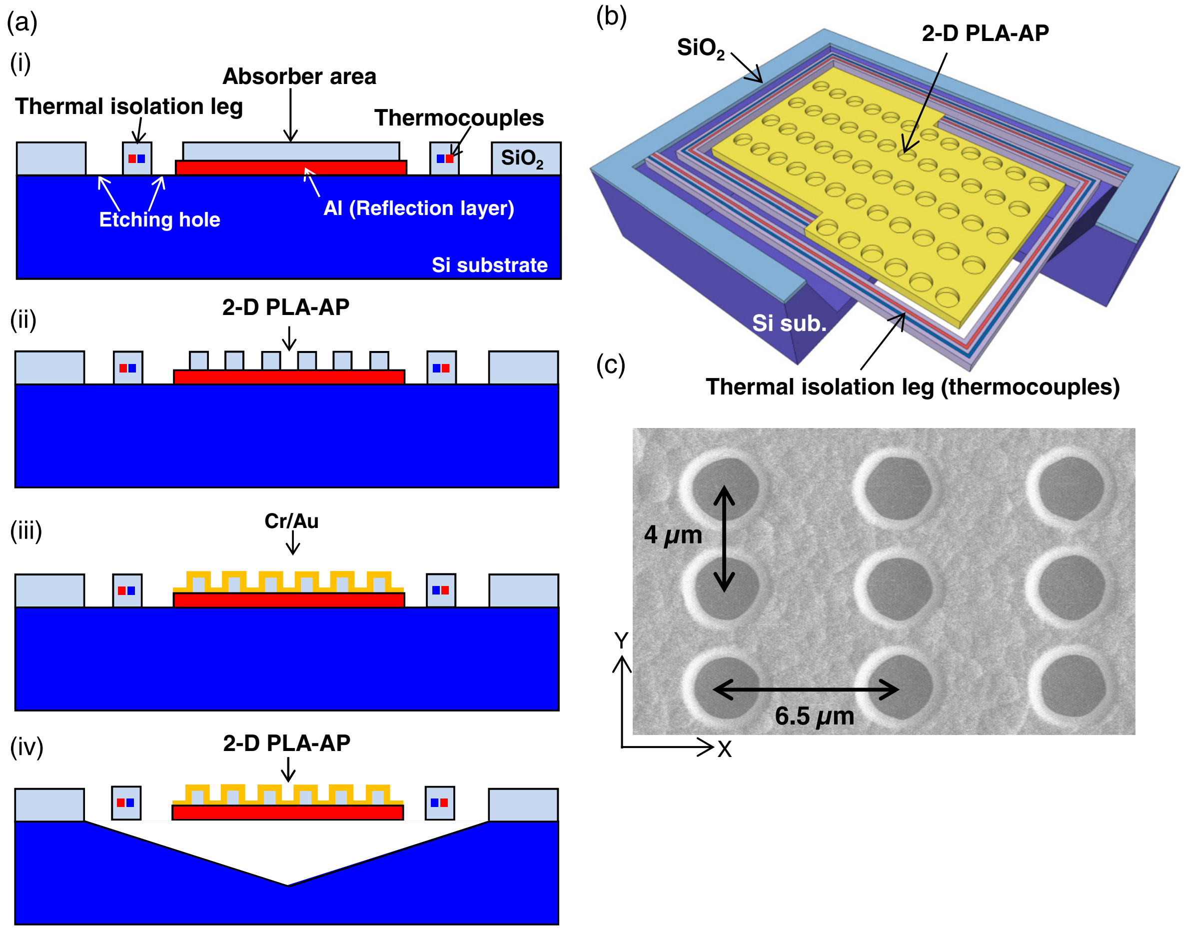

Fig. 4 (a) Procedure for the fabrication of an MEMS-based thermopile incorporating a 2-D PLA-AP. (b) Schematic diagram of the completed MEMS-based thermopile with 2-D PLA-AP. (c) SEM image of the 2-D PLA-AP surface.

with a Lorentzian function. The second resonance peak at $\omega = 1.22$ has an asymmetric line shape of Fano resonance, as shown in Fig. 3(f). This asymmetric line shape is produced because $c_1(\omega)$ becomes zero at $\omega = 1.2$ and $\gamma_2 = 0$ close to the second resonance peak at $\omega = 1.22$, which distorted the line shape of the resonance peak. This destructive interference corresponds to the absorption spectra of 2-D PLA-APs, where the surface plasmon resonance in the x-direction destructively interferes with that in the y-direction near its peak wavelength, which produces the asymmetric line shape of the absorption spectrum shown in Fig. 2.

3 Sensor Fabrication

Microelectromechanical systems (MEMS)-based uncooled IR sensors (or thermopiles) based on 2-D PLA-APs were subsequently fabricated. Figure 4(a) summarizes the fabrication process. This procedure and the thermopile were the same as those reported in our previous studies,[10,12] except that in the present case the 2-D PLA-APs were patterned on the IR absorber area.

Each device was fabricated on a 6-in. silicon substrate using a standard complementary metal oxide semiconductor (CMOS) process. The thermocouples consisted of a series of p- and n-type poly-Si regions, the resistivity of which was controlled by ion implantation. An Al layer was formed under the absorber area as a backside reflective layer, and holes serving as cavities were formed via reactive-ion etching (RIE). A 1.5-μm-thick SiO_2 layer was subsequently deposited on the absorber area. Following this, the 2-D PLA-AP structure was formed by RIE only on the SiO_2 layer of the IR absorber area. Next, 50- and 250-nm-thick Cr and Au layers were deposited by sputtering, where the Cr layer acted as an adhesive between the SiO_2 and Au layers. The 250-nm-thick Au layer was significantly thicker than the skin depth in the IR wavelength region, so the effects of the Cr and SiO_2 layers beneath Au were negligible. The Cr/Au layers were selectively etched using a wet etchant to reveal the holes previously covered by the sputtered Cr/Au. Scanning electron microscopy (SEM) observations confirmed that the Cr/Au layers were uniformly coated. Each wafer was then diced into chips and the Si was anisotropically etched through the holes using tetramethylammonium hydroxide (TMAH). The TMAH was doped with Si so that the reflective backside Al layer was not etched. The cavity under the IR absorber area was then formed to complete the thermally isolated freestanding structure. Figures 4(b) and 4(c) present a schematic diagram of the thermopile with incorporated 2-D PLA-AP and an SEM image of the 2-D PLA-AP surface. The detector area (300×200 μm) was surrounded by long thermal isolation legs to reduce thermal conductance.

4 Measurements and Discussion

The spectral responsivity of the sensor was measured for nonpolarized and polarized incident IR light using the same experimental setup as that used in our previous work.[10,12] Narrow-band filters were used to select the evaluation wavelengths, and the spectral responsivities were calculated according to the equations from Ref. 9. Figure 5 shows the measured spectral responsivity, which clearly demonstrates that this newly developed sensor operates as a dual-band detector for nonpolarized IR light, in which

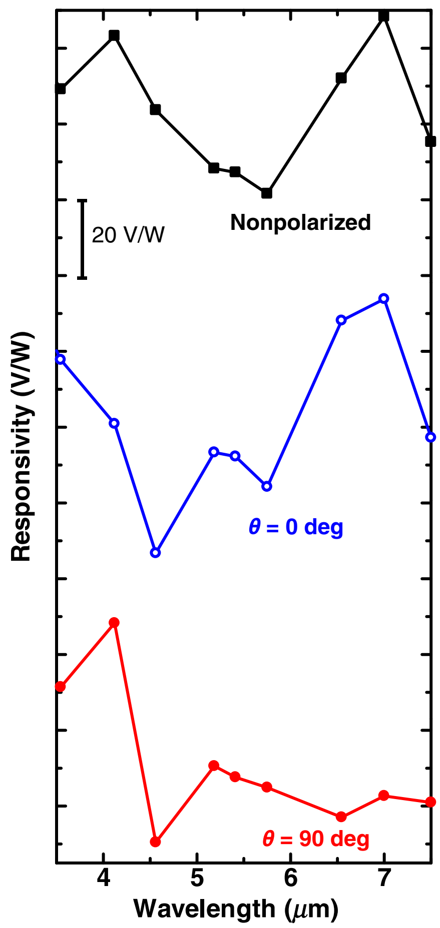

Fig. 5 Spectral responsivity of an uncooled IR sensor incorporating a 2-D PLA-AP with p_y and p_x of 4.0 and 6.5 μm, respectively; nonpolarization and polarization dependence of 0 deg and 90 deg. The scale bar represents 20 V/W.

the bands approximately correspond to the asymmetric periods p_x and p_y. Dual- and single-responsivity peaks were clearly observed for polarization with $\theta = 0$ deg and 90 deg. The asymmetry is attributed to Fano resonance, and the results are in agreement with the calculated results shown in Fig. 2. Dual-band operation was also demonstrated to represent the average responsivities of the convolution between polarization with $\theta = 0$ deg and 90 deg due to the independent nature of the incident IR. Our spectral resolution is not sufficient to precisely evaluate the peak responsivity. However, the difference between the maximum responsivity peak value and the minimum is at least 50 V/W, which is comparable to conventional thermopiles and is sufficient for practical applications. The responsivity can be further enhanced by optimizing the sensor structures, such as the absorber area, and the thermal isolation coefficient. Dual-band or single-mode operation can be selected according to the use of a nonpolarized or polarized light source, which is advantageous considering the total sensor systems.

5 Conclusions

A dual-band uncooled IR sensor was successfully developed using a 2-D PLA-AP. RCWA simulations showed that two asymmetric absorption peaks were produced by the 2-D

PLA-AP, according to the polarization angle of the incident IR. These asymmetric absorption spectra were well explained by the classical analogy of Fano resonance. The asymmetric line shape of the Fano resonance in 2-D PLA-APs is attributed to the destructive interference of the asymmetric surface plasmon resonance of the *x*- and *y*-directions. An MEMS-based thermopile was fabricated with the 2-D PLA-AP. The spectral responsivity for nonpolarized and polarized incident light of the developed sensor with the 2-D PLA-AP confirmed that dual-band operation was realized due to the polarization-dependent Fano resonance. Dual-band operation such as that exhibited by this device should be applicable to various types of thermal IR sensors, such as bolometers and silicon-on-insulator (SOI) diodes.[34] Thus, it is expected that the Fano resonance mode of the symmetry-broken plasmonic structures studied in this report will contribute to the development of advanced multimode uncooled IR sensors for various analysis applications.

Acknowledgments

The authors thank Masashi Ueno, Takahiro Ohanakado, and Tetsuya Satake of the Advanced Technology R&D Center of Mitsubishi Electric Corporation for helpful support.

References

1. P. W. Kruse, *Uncooled Thermal Imaging Arrays, Systems, and Applications*, SPIE Press, Bellingham, Washington (2001).
2. M. Kimata, "Trends in small-format infrared array sensors," in *Proc. Sensors*, pp. 1–4, IEEE (2013).
3. M. Vollmer and K.-P. Mollmann, *Infrared Thermal Imaging: Fundamentals, Research and Applications*, Wiley-VCH, Weinheim (2010).
4. Y. Ohtera and H. Yamada, "Photonic crystals for the application to spectrometers and wavelength filters," *IEICE Electron. Express* **10**(8), 20132001 (2013).
5. M. A. Vincenti et al., "Color control through plasmonic metal gratings," *Appl. Phys. Lett.* **100**(20), 201107 (2012).
6. B. Zeng, Y. Gao, and F. J. Bartoli, "Ultrathin nanostructured metals for highly transmissive plasmonic subtractive color filters," *Sci. Rep.* **3**, 2840 (2013).
7. Z. Li, A. W. Clark, and J. M. Cooper, "Dual color plasmonic pixels create a polarization controlled nano color palette," *ACS Nano* **10**(1), 492–498 (2016).
8. J. J. Talghader, A. S. Gawarikar, and R. P. Shea, "Spectral selectivity in infrared thermal detection," *Light Sci. Appl.* **1**(8), e24 (2012).
9. S. Ogawa et al., "Wavelength selective uncooled infrared sensor by plasmonics," *Appl. Phys. Lett.* **100**(2), 021111 (2012).
10. S. Ogawa et al., "Wavelength selective wideband uncooled infrared sensor using a two-dimensional plasmonic absorber," *Opt. Eng.* **52**(12), 127104 (2013).
11. D. Fujisawa et al., "Multi-color imaging with silicon-on-insulator diode uncooled infrared focal plane array using through-hole plasmonic metamaterial absorbers," in *28th IEEE Int. Conf. on Micro Electro Mechanical Systems (MEMS '15)*, pp. 905–908, IEEE (2015).
12. S. Ogawa et al., "Polarization-selective uncooled infrared sensor with asymmetric two-dimensional plasmonic absorber," *Opt. Eng.* **53**(10), 107110 (2014).
13. S. Ogawa, Y. Takagawa, and M. Kimata, "Polarization-selective uncooled infrared sensor using a one-dimensional plasmonic grating absorber," *Proc. SPIE* **9451**, 94511K (2015).
14. S. Kawata, "Plasmonics: future outlook," *Jpn. J. Appl. Phys.* **52**(1), 010001 (2013).
15. R. Stanley, "Plasmonics in the mid-infrared," *Nat. Photonics* **6**(7), 409–411 (2012).
16. D. R. Smith, J. B. Pendry, and M. C. Wiltshire, "Metamaterials and negative refractive index," *Science* **305**(5685), 788–792 (2004).
17. N. Meinzer, W. L. Barnes, and I. R. Hooper, "Plasmonic meta-atoms and metasurfaces," *Nat. Photonics* **8**(12), 889–898 (2014).
18. C. M. Watts, X. Liu, and W. J. Padilla, "Metamaterial electromagnetic wave absorbers," *Adv. Mater.* **24**(23), OP98-OP120 (2012).
19. F. Cheng et al., "Structural color printing based on plasmonic metasurfaces of perfect light absorption," *Sci. Rep.* **5**, 11045 (2015).
20. B. Zhang et al., "Polarization-independent dual-band infrared perfect absorber based on a metal-dielectric-metal elliptical nanodisk array," *Opt. Exp.* **19**(16), 15221–15228 (2011).
21. Q.-Y. Wen et al., "Dual band terahertz metamaterial absorber: design, fabrication, and characterization," *Appl. Phys. Lett.* **95**(24), 241111 (2009).
22. Y. B. Chen and F. C. Chiu, "Trapping mid-infrared rays in a lossy film with the Berreman mode, epsilon near zero mode, and magnetic polaritons," *Opt. Express* **21**(18), 20771–20785 (2013).
23. T. Maier and H. Brueckl, "Multispectral microbolometers for the midinfrared," *Opt. Lett.* **35**(22), 3766 (2010).
24. K. Masuda et al., "Optimization of two-dimensional plasmonic absorbers based on a metamaterial and cylindrical cavity model approach for high-responsivity wavelength-selective uncooled infrared sensors," *Sens. Mater.* **26**(4), 215–223 (2014).
25. Y. Takagawa, S. Ogawa, and M. Kimata, "Detection wavelength control of uncooled infrared sensors by two-dimensional lattice plasmonic absorbers," *Sensors* **15**(6), 13660–13669 (2015).
26. S. Ogawa, Y. Takagawa, and M. Kimata, "Dual-band uncooled infrared sensors employing Fano resonance in plasmonic absorbers," *Proc. SPIE* **9819**, 98191L (2016).
27. U. Fano, "Effects of configuration interaction on intensities and phase shifts," *Phys. Rev.* **124**(6), 1866–1878 (1961).
28. Y. S. Joe, A. M. Satanin, and C. S. Kim, "Classical analogy of Fano resonances," *Phys. Scr.* **74**(2), 259–266 (2006).
29. A. Christ et al., "Waveguide-plasmon polaritons: strong coupling of photonic and electronic resonances in a metallic photonic crystal slab," *Phys. Rev. Lett.* **91**(18), 183901 (2003).
30. A. Christ et al., "Optical properties of planar metallic photonic crystal structures: experiment and theory," *Phys. Rev. B* **70**(12), 125113 (2004).
31. N. Verellen et al., "Fano resonances in individual coherent plasmonic nanocavities," *Nano Lett.* **9**(4), 1663–1667 (2009).
32. B. Luk'yanchuk et al., "The Fano resonance in plasmonic nanostructures and metamaterials," *Nat. Mater.* **9**(9), 707–715 (2010).
33. P. Fan et al., "Optical Fano resonance of an individual semiconductor nanostructure," *Nat. Mater.* **13**(5), 471–475 (2014).
34. T. Maegawa et al., "2-in-1 diodes with a contact-sidewall structure for small pixel pitch in silicon-on-insulator (SOI) uncooled infrared (IR) focal plane arrays," *Sens. Mater.* **26**(4), 189–198 (2014).

Shinpei Ogawa received his BE, ME, and PhD degrees from the Department of Electronic Science and Engineering, Kyoto University, Japan, in 2000, 2002, and 2005, respectively. He has been with the Advanced Technology R&D Center, Mitsubishi Electric Corporation, Amagasaki, Japan, since 2005. He works on the development of various MEMS devices, including RF-MEMS switches, inductors, through-silicon vias, optical sensors, and infrared sensors. He is currently a unit leader of plasmonics, metamaterials, and graphene research.

Yousuke Takagawa received his BE and ME degrees from the College of Science and Engineering, Ritsumeikan University, Japan, in 2013 and 2015, respectively. He has been with Mitsubishi Electric Corporation, Japan, since 2015.

Masafumi Kimata received his MS degree from Nagoya University in 1976 and received his PhD degree from Osaka University in 1992. He joined Mitsubishi Electric Corporation in 1976 and retired from Mitsubishi Electric in 2004. Currently, he is a professor at Ritsumeikan University, where he continues his research on MEMS-based uncooled infrared focal plane arrays and type-II superlattice infrared focal plane arrays. He is a fellow of SPIE.